

Anisotropic displacement threshold energy and defect distribution in diamond: PKA energy and temperature effect

Ke Wu(吴可), Zeyi Du(杜泽依), Hongyang Liu(刘洪洋), Nanyun Bao(包南云), Chengke Xu(许成科), Hongrui Wang(王泓睿), Qunchao Tong(童群超), Bo Chen(陈博), Dongdong Kang(康冬冬), Guang Wang(王广), and Jiayu Dai(戴佳钰)

Citation: Chin. Phys. B, 2025, 34 (**8**): 087104. DOI: 10.1088/1674-1056/add4f8
http://cpb.iphy.ac.cn; http://iopscience.iop.org/cpb

What follows is a list of articles you may be interested in

Atomistic simulations of graphene origami: Dynamics and kinetics

Panpan Zhang(张盼盼), Haihong Jia(贾海洪), Yan-Fang Zhang(张艳芳), and Shixuan Du(杜世萱)
Chin. Phys. B, 2023, 32 (**8**): 087107. DOI: 10.1088/1674-1056/acd527

Robust and intrinsic type-III nodal points in a diamond-like lattice

Qing-Ya Cheng(程青亚), Yue-E Xie(谢月娥), Xiao-Hong Yan(颜晓红), and Yuan-Ping Chen(陈元平)
Chin. Phys. B, 2022, 31 (**11**): 117101. DOI: 10.1088/1674-1056/ac7c00

Magnetic and electronic properties of two-dimensional metal-organic frameworks $TM_3(C_2NH)_{12}$

Zhen Feng(冯振), Yi Li(李依), Yaqiang Ma(马亚强), Yipeng An(安义鹏), and Xianqi Dai(戴宪起)
Chin. Phys. B, 2021, 30 (**9**): 097102. DOI: 10.1088/1674-1056/ac0cdb

First-principles study on the mechanics, optical, and phonon properties of carbon chains

Jin-Ping Li(李金平), Song-He Meng(孟松鹤), Han-Tao Lu(陆汉涛), Takami Tohyama(遠山貴巳)
Chin. Phys. B, 2018, 27 (**11**): 117101. DOI: 10.1088/1674-1056/27/11/117101

Modeling of metal-oxide semiconductor：Analytical bond-order potential for cupric oxide

Li Kun (李坤), Yang Wen (杨雯), Wei Ji-Lin (魏计林), Du Shi-Wen (杜诗文), Li Yong-Tang (李永堂)
Chin. Phys. B, 2014, 23 (**4**): 047103. DOI: 10.1088/1674-1056/23/4/047103

Anisotropic displacement threshold energy and defect distribution in diamond: PKA energy and temperature effect

Ke Wu(吴可)[1], Zeyi Du(杜泽依)[1], Hongyang Liu(刘洪洋)[1], Nanyun Bao(包南云)[1], Chengke Xu(许成科)[1], Hongrui Wang(王泓睿)[1], Qunchao Tong(童群超)[1,2,3,†], Bo Chen(陈博)[1,2,3], Dongdong Kang(康冬冬)[1,2,3], Guang Wang(王广)[1], and Jiayu Dai(戴佳钰)[1,2,3,‡]

[1] *College of Science, National University of Defense Technology, Changsha* 410073, *China*
[2] *Hunan Key Laboratory of Extreme Matter and Applications, National University of Defense Technology, Changsha* 410073, *China*
[3] *Hunan Research Center of the Basic Discipline for Physical States, National University of Defense Technology, Changsha* 410073, *China*

(Received 20 February 2025; revised manuscript received 28 April 2025; accepted manuscript online 7 May 2025)

Diamond is a promising semiconductor material for future space exploration, owing to its unique atomic and electronic structures. However, diamond materials and related devices still suffer from irradiation damage under space irradiation involving high-energy irradiating particles. The study of the generation and evolution of point defects can help understand the irradiation damage mechanisms in diamond. This study systematically investigated the defect dynamics of diamond in 162 crystallographic directions uniformly selected on a spherical surface using molecular dynamics simulations, with primary knock-on atom (PKA) energies up to 20 keV, and temperatures ranging from 300 K to 1800 K. The results reveal that the displacement threshold energy of diamond changes periodically with crystallographic directions, which is related to the shape of potential energy surface along that direction. Additionally, the number of residual defects correlates positively with PKA energy. However, temperature has dual competing effects: while it enhances the probability of atomic displacement, it simultaneously suppresses the probability of defect formation by accelerating defect recombination. The calculation of sparse radial distribution function indicates that the defect distribution shows a certain degree of similarity in the short-range region across different PKA energies. As the PKA energy increases, defect clusters tend to become larger in size and more numerous in quantity. This study systematically investigates the anisotropy of displacement threshold energy and elucidates the relationship between various irradiation conditions and the final states of irradiation-induced defects.

Keywords: displacement cascades, diamond, molecular dynamics, temperature effect

PACS: 71.15.Pd, 61.80.Lj

DOI: 10.1088/1674-1056/add4f8 **CSTR:** 32038.14.CPB.add4f8

1. Introduction

Diamond possesses unique physical properties, including high thermal conductivity, ultrawide band gap, high carrier mobility, and excellent radiation resistance.[1–10] Due to the radiation resistance, diamond has extensive applications in irradiated environments, including radiation detectors for particle accelerators and nuclear detection,[11] medical dosimeters,[12] x-ray mirrors,[13–15] and windows in high-power optics. However, despite its inherent radiation resistance, diamonds can still experience property degradation due to strong irradiation, which introduces various defects during exposure to high-energy particles such as protons and heavy ions.[16–18] Therefore, it is necessary to study the irradiation damage mechanisms of diamonds to guide the application of diamond devices.

When diamond devices are exposed to a radiation environment, displacement cascades are induced by incident energetic particles.[19,20] These cascades lead to the production of point defects, such as interstitials and vacancies, which can further aggregate into clusters or voids. As defects accumulate, carrier mobility diminishes, indicating that structural damage can impair the performance of the device.[21] To ensure the long-term reliable performance of diamonds in a radiation environment, it is essential to understand the defect generation and residual conditions in detail. Experimentally, photoluminescence technology,[22] cathode luminescence technology,[23] transmission electron microscopy,[24] Raman spectroscopy,[25,26] scanning electron microscopy,[27] and x-ray diffraction[15] can be employed for structure analysis. However, experimentally observing defects in real-time is extremely challenging since displacement cascades occur over nanometer-length scales and picosecond (ps) timescales. Fortunately, molecular dynamics (MD) simulations provide a complementary approach to tracing the atomic movement in materials under external forces, such as laser or pressure.[28,29] Owing to the rapid advancement of computing power, irradiation damage has been investigated using molecular dynamics simulations.[30–36]

The threshold displacement energy (E_d) is defined as the

†Corresponding author. E-mail: tongqunchao@nudt.edu.cn
‡Corresponding author. E-mail: jydai@nudt.edu.cn

© 2025 Chinese Physical Society and IOP Publishing Ltd. All rights, including for text and data mining, AI training, and similar technologies, are reserved.

minimum energy needed to displace the primary knock-on atom (PKA) sufficiently from its lattice site and form a vacancy and interstitial (Frenkel) pair,[37–39] which is a fundamental parameter for determining the radiation tolerance of a material. On the one hand, E_d correlates the kinetic energy of an incident particle or PKA with the number of defects generated through cascade collisions.[40] On the other hand, the displacement threshold energy must be specified in advance in the mesoscopic simulation of material radiation damage.[41]

Constrained by temporal and spatial resolution limitations, experimental techniques are unable to accurately determine the displacement threshold energy along various crystallographic directions. Currently, MD have been used to study the E_d of low-index crystal directions in diamonds. Wu *et al.* simulated that the E_d for $\langle 100\rangle$, $\langle 110\rangle$, and $\langle 111\rangle$ crystal directions in diamond is approximately 50 eV,[42] which is higher than that of other semiconductors (about 25 eV).[43,44] Erginsoy *et al.* explored the concept of displacement probability, highlighting that exceeding the E_d does not ensure defect formation.[45] Considering the probabilistic nature of the E_d, Delgado *et al.* carried out extensive simulations for three low-index crystal directions in diamond and performed hundreds of trials to construct the displacement probability curve,[46] their results indicated that the E_d of diamond along three crystal directions ranges between 30 eV and 100 eV. However, since the randomness of the cascade collision can cause atomic velocities in any direction, it is crucial to systematically investigate the displacement threshold energy for a broader range of crystal directions in diamond. With respect to the PKA energy effect, some studies on diamond cascade collisions revealed that when the PKA energy reaches up to 5 keV, the collision cascades are of short duration (femtosecond, fs) and exhibit fractal trajectories.[42,47,48] In the temperature effect, Liu *et al.* simulated that as the temperature increases, the number of defects in the final state of diamond cascade collisions decreases.[49] In the distribution of residual point defect, current research primarily focuses on the distance between the farthest two point defects.[48,50] In summary, the displacement threshold energies of diamond along various crystallographic directions, as well as the interplay between broad PKA energy and temperature ranges and their influence on point defect generation, evolution, residual defect numbers, residual defect distributions, and defect clustering, remain underexplored. Further in-depth and detailed analysis is imperative to fully elucidate these intricate relationships.

In this study, we explore the defect generation and residual condition of diamond under a broad range of irradiation conditions, specifically across temperatures from 300 K to 1800 K and PKA energies up to 20 keV. By extending the simulation scenarios to a wider range of parameters, this research substantially enhances our understanding of diamond behavior under irradiation. To fully investigate the displacement threshold energy of diamonds, we systematically studied 162 different crystallographic directions. The atom displacement probability (DP) and defect formation probability (DFP) were statistically calculated under various PKA energies and temperatures. Additionally, we explored the mechanism of temperature on the diamond cascade collision process by analyzing how different temperatures affect the DP and DFP values. The defect recombination rate and sparse radial distribution function is used to analyze the final state of defects. The defect cluster under different PKA energies and temperatures are also discussed. The remainder of this paper is organized as follows. Section 2 addresses the methodology of MD simulations and data analysis, followed by results and detailed discussion on defects in Section 3. Conclusions are presented in Section 4.

2. Theoretical methods

All molecular dynamics simulations were conducted using the large-scale atomic/molecular massively parallel simulator (LAMMPS) code. The Tersoff-ZBL potential has been employed to describe the elasticity constant, interstitial formation energy, and vacancy formation energy of diamond, while also accounting for the short-range interactions between carbon atoms during cascade collisions.[51,52] The accuracy of this potential is detailed in the supplementary information S1.

In the MD simulation, the energy of the system is first minimized, followed by a relaxation period within the isothermal–isobaric ensemble (NPT) for 2.5 ps, with a time step of 1 fs. Notably, in the simulation of irradiation displacement damage, the interaction of energetic particles with the diamond lattice is modeled as a sudden localized input of kinetic energy into the PKA. Once the irradiated particle transfers its energy to the PKA, its role can be neglected. Only the cascade collision process initiated by the PKA within the lattice is considered. The system is then relaxed within the micro-canonical ensemble (NVE) over 15 ps using variable time steps. The maximum distance allowed for atomic movement in each time step is limited to 0.018 Å. This approach is necessary due to the light mass of carbon atoms, which results in high velocities when imparted with kinetic energy. The size of the simulation system is listed in Table S3. To simulate the external ambient temperature, a thermostat layer was modeled in a region at a distance of 3.57 Å from the supercell boundary and connected to a Nosé–Hoover thermostat. To confine each collision cascade within the cubic supercell, the location of the PKA were selected such that the cascade would evolve towards the center of the cell, and the displaced atoms will not move to the boundary of the simulation cell. The atomic structure and defect configuration are visualized using the Open Visualization Tool (OVITO).[53] The Wigner–Seitz method was applied to

identify the Frenkel pairs and cluster analysis modifiers were used to analyze the clusters for these point defects.

3. Results and discussion

3.1. Displacement threshold energy

The E_d along the low-index crystallographic directions of diamond has been studied using various methods. Here, we conducted a comprehensive calculation of the E_d in diamond, taking into account both its probability and anisotropy. For each direction, we performed three simulations where the PKA energy was varied from 20 eV to 100 eV. Therefore, a total of 240 simulations were performed for each PKA crystal orientation. The displacement threshold energy was defined as the minimum PKA energy required to form a stable defect. For low-energy atomic cascade collisions, an $10\times10\times10$ supercell containing 8000 atoms was used. The simulation was conducted at a temperature of 300 K, 900 K, and 1500 K. The PKA was positioned at the center of the simulation box. MD cascade collision simulations were performed along 162 unique directions, which were uniformly distributed across the unit sphere. The energy of PKA was incrementally increased during simulations.

The PKA directions were determined by the angles θ and ϕ, where θ represents the angle between the PKA direction and the c-axis, and ϕ denotes the angle between the projection of the PKA direction onto the a–b plane and the a-axis, as shown in Fig. 1(a). θ ranges from 0° to 180°, and ϕ ranges from 0° to 360°, the PKA directions were taken at intervals of 20° across both angles. A total of 38880 cascade simulations were performed.

Figure 1(b) shows the E_d of diamond as a function of the PKA incident angle. The E_d for various crystallographic directions in diamond ranges from 31 eV to 72 eV, revealing a clear correlation with the incident angle of the PKA. Our results are within the range of experimental and calculated values (about 30 eV–100 eV) reported in the literature.[46,54–56] From lattice symmetry perspective, diamond has cubic symmetry and belongs to the O_h point group, which means the reference a and c-axis we selected are the C_2 rotation symmetry axis (Even though the a-axis and c-axis are also C_4 rotation symmetry axis, the C_4 in the diamond structure involves a combination of rotation and translation, rather than pure rotation.). Therefore, the E_d of the PKA on the spherical surface exhibits periodic behavior, completing a full variation cycle as θ and ϕ ranges from 0° to 180° . From a static calculation perspective, the displacement threshold energy is related to the shape of the potential energy surface along that crystallographic direction. Typically, the higher the potential barrier at the equilibrium position, the greater the displacement threshold energy (see supplementary information S3 for details).

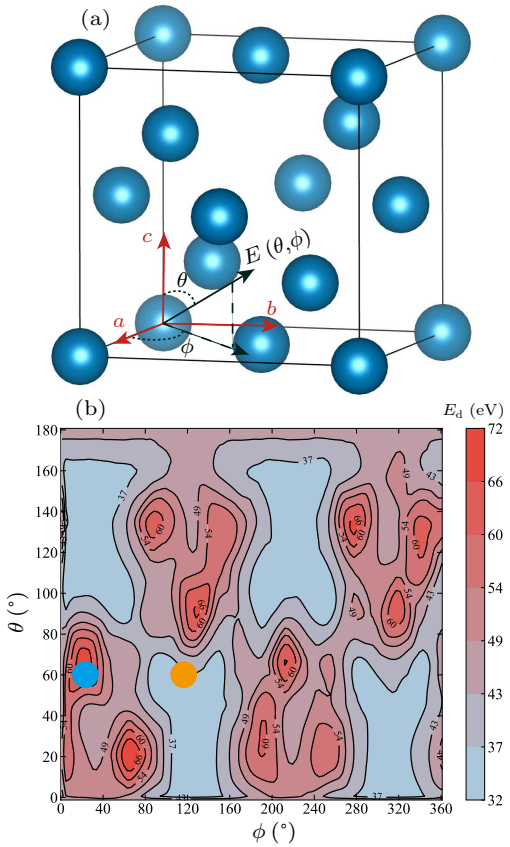


Fig. 1. (a) Schematic diagram of the unit cell illustrating the different incidence directions of PKAs, (b) displacement threshold energy for different incidence directions of PKAs at 300 K in diamond.

To further understand the relationship between the generation of point defects and the direction of the PKA as well as temperature. We selected two directions, one with a higher E_d ($\theta = 60°$ and $\phi = 20°$) and another with a lower E_d ($\theta = 60°$ and $\phi = 100°$), to calculate the potential energy of the system as the PKA with an energy of 50 eV. The results are illustrated in Fig. 2, in which the arrows in the inset indicate the displacement of atoms relative to their equilibrium positions, and the color of the atoms represents their atomic energy. After acquiring kinetic energy, the PKA begins to move along a specific direction, departing from its equilibrium position. During this process, the PKA continuously consumes its kinetic energy to overcome potential barriers, leading to a rapid increase in the potential energy of the system, as shown from 0 to 0.02 ps in Fig. 2. If the PKA encounters another neighboring potential well before its kinetic energy is exhausted and the temperature is low enough that the thermal kinetic energy of the PKA is less than the depth of the neighboring well, it can be captured and will vibrate within this potential well. Meanwhile, the potential energy of the system decreases, as illustrated in the direction with ($\theta = 60°$ and $\phi = 100°$) in Fig. 2, eventually leading to the formation of a $\langle 100 \rangle$ split interstitial defect (see Table S1 and Fig. S1 for details). On the contrary, if no other potential well is encountered before the PKA's kinetic energy is depleted, the PKA will return to its initial equilibrium position under the driving of atomic forces, as shown in direction

with ($\theta = 60°$ and $\phi = 20°$). Compared to the scenario where a defect is formed, the potential energy of the system decreases more significantly in this case. The variation of the system's potential energy along more directions is shown in Fig. S5 in the supporting information and these crystallographic directions also conform to the aforementioned physical picture. For comparison, figure S6 shows the variation of the system's potential energy along the direction of ($\theta = 60°$ and $\phi = 20°$) when the PKA energy is 50 eV and 80 eV. As expected, only the 80 eV PKA can overcome the potential barrier to form a stable defect.

Figure 2 shows that atoms are displaced in both two directions, but only one direction ultimately produces a stable defect. Therefore, we emphasize that the displacement threshold energy involves the displacement, diffusion, and recombination of atoms, which is a physical process spanning multiple temporal and spatial scales. Meanwhile, the potential barrier and well along the direction of PKA movement, as one factor, can influence atomic diffusion and exhibits a certain correlation with the displacement threshold energy.

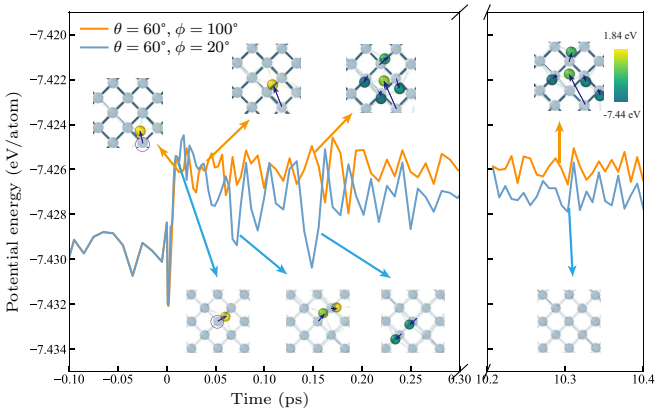


Fig. 2. The potential energy of the system varies with time, in which PKA direction is along $\theta = 60°$, $\theta = 100°$; $\theta = 60°$, $\phi = 20°$. The moment when the PKA acquires energy is set as time zero. The arrows in the inset indicate the displacement of atoms relative to their equilibrium positions. Atoms that have not deviated from their equilibrium positions are set to be transparent and the color of the displacement atoms represents their atomic energy.

To understand the intrinsic randomness of E_d and the effects of temperature and PKA energy on defect formation, the atom displacement probability (DP) and defect formation probability (DFP)[57] in 300 K, 900 K, and 1500 K were calculated as shown in Fig. 3. The following methods were employed to obtain the DP and DFP. When the PKA energy is 40 eV, atomic displacements were observed in 97 PKA directions, and 68 PKA directions generate stable defects, therefore, DP = 97/162 = 0.5988, DFP = 68/162 = 0.4198. Each PKA energy, direction, and temperature were simulated three times independently, and each data point in Fig. 3 was an average across all PKA directions, representing 486 MD simulations.

The DP captures both defect formation and atomic replacement events and as expected, it converges to unity much more rapidly than the DFP as shown in Fig. 3. As the PKA energy increases, both DP and DFP increase. Once the PKA energy exceeds 50 eV, the energetic PKA will invariably cause displacement, leading to the transient formation of point defects. Consequently, the probability of atomic displacement reaches 100%. This indicates that an energy of 50 eV is sufficient to cause carbon atoms in diamond to leave their lattice equilibrium positions.

Under the same PKA energy the value of DFP is consistently lower than DP. This phenomenon can be attributed to the fact that once atoms acquire sufficient energy to escape from their equilibrium positions, and enter interstitial sites. However, there are no potential wells to trap atoms and form stable defects, before the kinetic energy of PKA is exhausted. Consequently, the interstitial atoms will return to its initial equilibrium position. Hence, not all displaced atoms will ultimately lead to the formation of stable point defects.

Figure 3 illustrates that temperature affects both the DP and the final DFP, with a more pronounced impact on DFP. When PKA energy is below 50 eV, the general trend suggesting an increased DP at higher temperatures. Higher temperatures elevate the vibrational energy of atoms and increase the likelihood of atomic displacement. However, as temperature increase, the DFP decreases significantly. This is because higher temperatures enhance the ability of atoms to overcome potential barriers and diffusion, thereby increasing the probability of recombination of point defects.

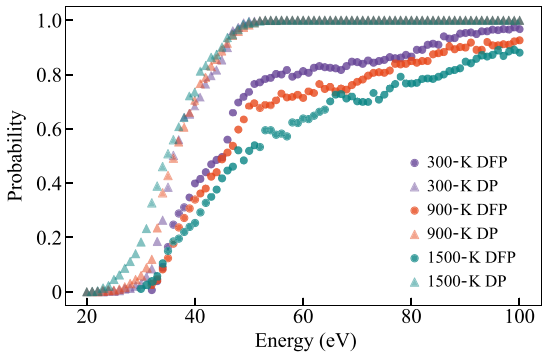


Fig. 3. Variation in DFP and DP with the PKA energy in 300 K, 900 K, and 1500 K

Hence, temperature effect on defects includes two competing mechanisms with opposing influences. On the one hand, higher temperature facilitates atomic displacement. On the other hand, it promotes the recombination of point defects. It is clear that both the thermal kinetic energy and the kinetic energy transferred by irradiation particles enhance the PKA's ability to overcome potential barriers. However, excessively high temperatures can increase the likelihood of the PKA overcoming the neighboring potential barrier, thereby increasing the probability of defect recombination. Hence, with the increase in temperature, there is a tendency for the displacement threshold energy in diamond to increase (see sup-

plementary information S3 for details). It is important to note that compared to the kinetic energy transferred by irradiation particles, the thermal kinetic energy caused by temperature is relatively small (at 300 K, the thermal kinetic energy is only about 0.03 eV). In summary, the initial energy of the PKA primarily determines its ability to overcome the potential barrier at the equilibrium position, while temperature mainly influences its ability to overcome the neighboring potential barrier.

3.2. Cascade collision process

The diamond ⟨110⟩ plane, which exhibits the lowest surface energy among all unreconstructed low-index crystal planes, can be regarded as the most stable.[58] Therefore, we selected the PKA along the ⟨110⟩ crystal direction with a moderate displacement threshold energy. In the irradiation damage simulations, the temperature ranges from 300 K to 1800 K, and the PKA energy ranges from 1 keV to 20 keV. To account for the inherent randomness in the cascade collision process, we performed 10 independent simulations for each set of conditions.

Figure 4(a) shows the number of residual defects exhibits a strong linear dependence on the PKA energy. This pattern coincides with the Norgett–Robinson–Thomson (NRT) model, in which the E_{d} is the key parameter relating the PKA energy to the number of defects.[40] The evolution of the number of defects with different energies of PKA can be found in Fig. S7. The peak number of defects at various temperatures remains largely consistent, as shown in Fig. S8. However, the quantity of residual defect tends to decrease with increasing temperature.

The work of Buchan *et al*. showed that the ratio of point defects to displaced atoms is independent of PKA energy.[48] However, the number of displaced atoms is insufficient to describe the degree of damage after irradiation, due to the probability that the displaced interstitial atoms have the chance to recombine with the vacancy defects during the annealing stage of the irradiation process. The defect recombination rate φ, which considers both the number of residual defects and the peak defect number, provides a comprehensive measure of the defect dynamics. Therefore, we used defect recombination rate as a reference to evaluate the resistance of radiation damage in diamond. The definition of φ is as follows, with its value ranging between 0 to 1.

$$\varphi = \frac{N_{\mathrm{peak}} - N_{\mathrm{final}}}{N_{\mathrm{peak}}},$$

where N_{peak} is the peak value of the number of defects, and the N_{final} denotes the number of residual defects. Figure 4(b) illustrates the variation of the defect recombination rate with temperature ranging from 300 K to 1800 K, for different PKA energies of 1 keV, 5 keV, 10 keV, and 20 keV. As the temperature increases, the defect recombination rate also increases, indicating a stronger tendency for defects to recombine at higher temperatures. This temperature-dependent behavior plays a crucial role in determining the dynamics of defect evolution and the final defect structure following irradiation.

Usually, the self-aggregation barriers for both interstitial (1.69 eV) and vacancy (2.46 eV) point defects are higher than the recombination barrier for interstitial-vacancy clusters (0.75 eV–1.01 eV).[26,59,60] Hence, an increase in temperature is more likely to lead to the recombination of interstitial and vacancy defects. On the other hand, as illustrated in Fig. 4(b), defect recombination rate decreases with increasing PKA energy. As the PKA energy increases, the peak number of defects increases (see supplementary information S5). However, the number of defects that recombine during the annealing stage is essentially the same (5 keV–20 keV). This implies that the higher PKA energy poses a greater challenge in repairing displacement damage.

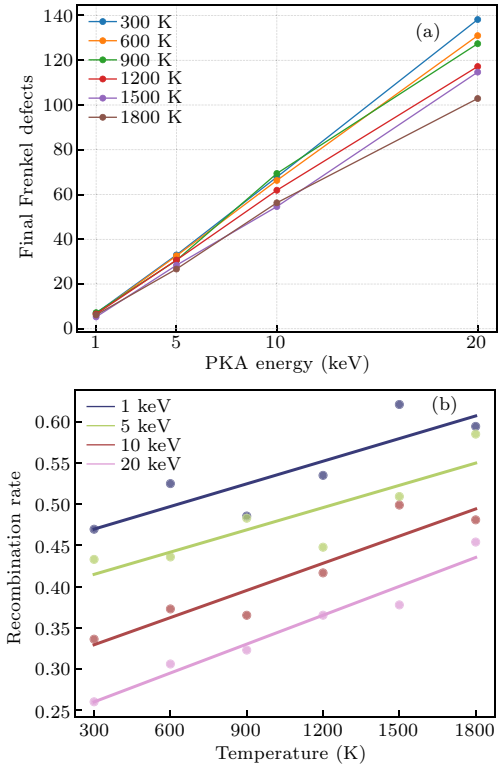


Fig. 4. (a) The variation of the number of residual defects in diamond with PKA energy at different temperatures. (b) The variation of the defect recombination rate with temperature at different PKA energies. The colored lines are fitted for better visualization.

To analyze the defect distribution in the final state of a cascade collision, the sparse radial distribution function, $g_{\mathrm{s}}(r)$ is calculated,[61] which defined as

$$g_{\mathrm{s}}(r) = \frac{2!\,(N-2)!}{N!} \sum_{i=1}^{N-1} \sum_{j>i}^{N} \delta(r_{ij} - r),$$

$$I_{\mathrm{s}}(r) = \int_0^r g_{\mathrm{s}}(x)\,\mathrm{d}x, \quad I_{\mathrm{s}}(\infty) = 1,$$

where N is the number of defects of interest. The notation $g_{\mathrm{s}}(r)$ is similar to the radial distribution function $g(r)$ but for

a sparse distribution (so labeled by the subscript "s"). With the definition, a quantity $(N_F - 1)g_s(r)$ denotes the average number of neighboring point defects at a distance r from a defect. N_F is the number of surviving Frenkel pairs. The plots of $(N_F - 1)g_s(r)$ for interstitials and vacancies in 300 K are shown in Figs. 5(a) and 5(b). For visualization, the y-axis benchmarks for different PKA energies have been offset from each other.

From Fig. 5, it can be observed that the distribution of vacancy defects and interstitial defects both broaden with increasing PKA energy. This is due to the fractal and branching characteristics of diamond point defect structures.[48] The higher the PKA energy, the longer the trajectory of the PKA in diamond, resulting in a wider defect distribution. Moreover, apart from some peaks at specific locations, the defect distribution caused by low-energy PKA shows certain similarities to that caused by high-energy PKA in the short-distance range, which could be attributed to the high symmetry of the diamond structure. Compared with PKA energy of 1 keV, new peaks appear at the position of 2.5 Å when the PKA energy is 5 keV, 10 keV, and 20 keV. Clearly, the formation of these point defects is due to the higher PKA energy, which transfers more kinetic energy to the neighboring atoms, enabling them to overcome the energy barrier and form stable defects. Finally, compared with the distribution of interstitial defects, the distribution of vacancy defects is shifted to the left as a whole and is mainly concentrated in the short-distance range. This is because the formation energy of vacancy defects is lower than that of interstitial defects, causing vacancy defects to tend to aggregate, while interstitial defects prefer to maintain a certain distance.

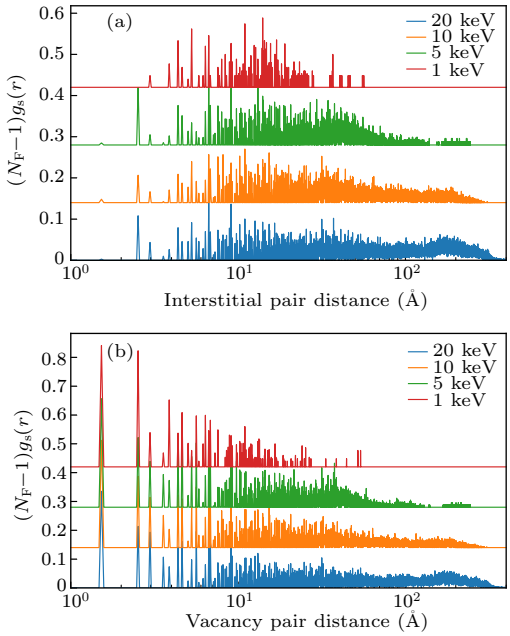


Fig. 5. Sparse radial distribution function $(N_F - 1)g_s(r)$ at 300 K, for (a) interstitials and (b) vacancies.

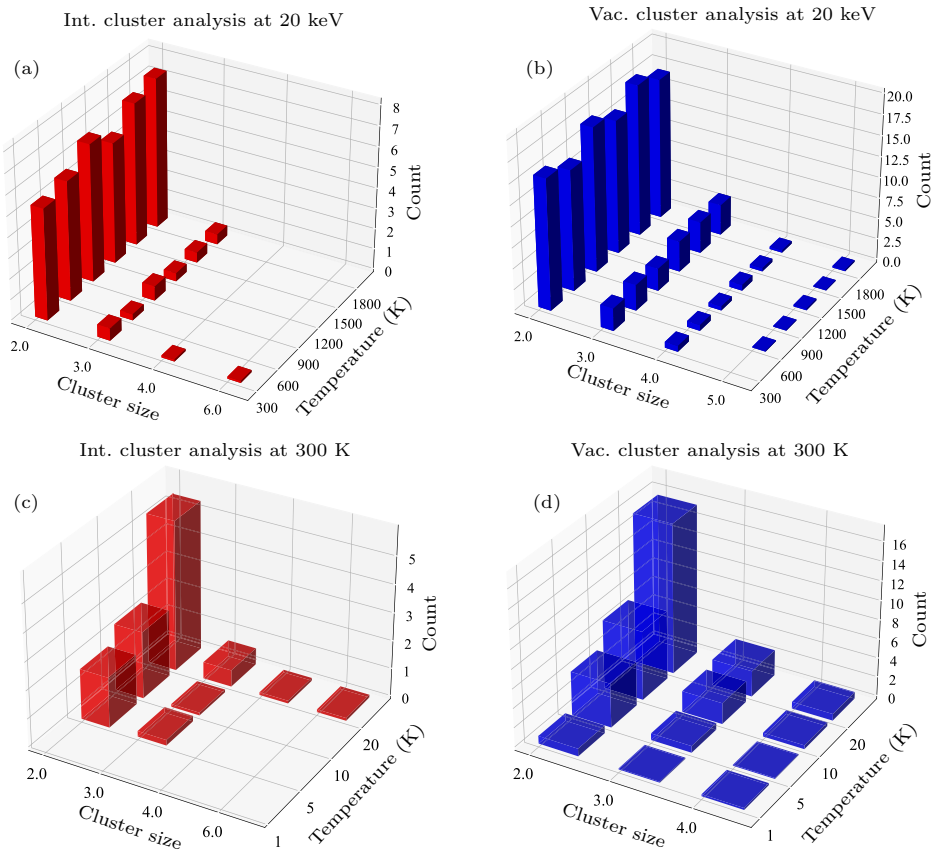


Fig. 6. The number of clusters as a function of PKA energy, temperature and size. (a) 20 keV for interstitial (Int.) clusters, (b) 20 keV for vacancy (Vac.) clusters, (c) 300 K for interstitial clusters, (d) 300 K for vacancy clusters.

Besides, for vacancy defects, the peak of $(N_F - 1)g_s(r)$ occurs at the nearest-neighbor distance (1.54 Å) for PKA energies ranging from 1 keV to 20 keV. This distribution characteristic may be related to the fact that the formation energy of the nearest-neighbor divacancy defect cluster is the lowest among defect clusters (see supplementary information S1 for details).

Defect clusters, as a product of the evolution of point defects, represent another important type of defect. The criterion for defining defect clusters is that if there are other interstitial defects within the second-nearest-neighbor distance (2.52 Å) around an interstitial defect, it is considered an interstitial cluster, and if there are other vacancy defects within the nearest-neighbor distance (1.54 Å) around a vacancy defect, it is considered a vacancy cluster (see supporting information S6 for details).[62] As illustrated in Fig. 6, the number of interstitial and vacancy clusters increases as PKA energy increase. However, the effect of temperature on the size and number of defect clusters does not show a clear trend within the temperature range of our simulations. The number of vacancy clusters is relatively higher than that of interstitial clusters. This discrepancy arises because the formation energy of vacancy clusters is lower, making them more energetically favorable. The formation energy for defect clusters is provided in Table S2 in supporting information. Upon completion of the diamond cascade collision process, the residual defect distribution from radiation damage is predominantly characterized by point defects, rather than the dislocation lines and loops that are typically observed in materials such as tungsten. This phenomenon arises from the lightness of carbon atoms. When carbon atoms are imparted with greater energy, they achieve higher velocities, which in turn lead to a defect distribution characterized by a branching pattern (see supporting information S7 for details).

4. Conclusions

In summary, we have comprehensively simulated the displacement threshold energy of diamond across 162 different directions and explored the cascade collision process in diamond over a wide range of conditions, including temperatures from 300 K to 1800 K and primary knock-on atom energies from 1 keV to 20 keV. These simulations were conducted using molecular dynamics methods based on the Tersoff-ZBL potential. Our results demonstrate that the displacement threshold energy varies periodically with crystal orientation, and its magnitude is associated with the shape of potential energy surface along the direction of PKA movement. Additionally, it is demonstrated that high PKA energy increases the number of residual defects; however, high temperature can reduce the number of residual defects by enhancing atomic diffusion capability. Finally, as the PKA energy increases, defect clusters tend to become larger in size and more numerous in quantity. The number of vacancy clusters is relatively higher than that of interstitial clusters due to the lower formation energy of vacancy clusters. This study systematically investigates the anisotropy of displacement threshold energy and elucidates the relationship between various irradiation conditions and the final states of irradiation-induced defects. It is worth emphasizing that, due to the limitations of the simulation methods, the electronic stopping effect during the displacement cascade process has not been considered in the current research. As a further research, we plan to develop a displacement cascade simulation method that considers the electronic stopping effect for wide-bandgap semiconductors, based on the two-temperature model or the electron-phonon model.

Acknowledgements

Project supported by the Science and Technology Innovation Program of Hunan Province, China (Grant No. 2021RC4026), the National Natural Science Foundation of China (Grant Nos. 12204538, 12104507, and 92365203), and Hunan Provincial Science Fund for Distinguished Young Scholars (Grant No. 2022JJ10060).

References

[1] Zamboni I, Pastuović Ž and Jakšić M 2013 *Diam. Relat. Mater.* **31** 65
[2] Pearton S, Aitkaliyeva A, Xian M, Ren F, Khachatrian A, Ildefonso A, Islam Z, Rasel M A J, Haque A and Polyakov A Y 2021 *ECS J. Solid State Sci. Technol.* **10** 055008
[3] Xu J, Dai J, Ren F Z, Wang Y F, Wang P, Xu S S, Wu S D, Lin J J, Yang Y and Guo D J 2021 *Carbon* **182** 525
[4] Zhou C, Liu Z J, Dou X L, Wu L, Guo Y, Li Z G and Zhang C R 2025 *Vacuum* **233** 113935
[5] Wang Y and Sun B 2024 *Appl. Phys. Lett.* **125** 042202
[6] Zheng Y H, Lu S H and Hu X J 2024 *Carbon* **226** 119210
[7] Rezek B, Watanabe H and Nebel C E 2006 *Appl. Phys. Lett.* **88** 042110
[8] Rogalin V E, Ashkenazi E E, Popovich A F, Ralchenko V G, Konov V I, Aranchii S M, Ruzin M V and Uspenskii S A 2012 *Russ. Microelectron* **41** 464
[9] Long Z M, Ben X Y, Jun W L and Bei G B 2005 *Chin. Phys. Lett.* **22** 1264
[10] Xu B and Tian Y J 2020 *Matter Radiat. at Extremes* **5** 068103
[11] Manfredotti C 2005 *Diam. Relat. Mater.* **14** 531
[12] Trucchi D M, Allegrini P, Calvani P, Galbiati A, Oliver K and Conte G 2012 *IEEE Electron Dev. Lett.* **33** 615
[13] Hirao N, Kawaguchi S I, Hirose K, Shimizu K, Ohtani E and Ohishi Y 2020 *Matter Radiat. at Extremes* **5** 68
[14] Zeng Q S 2023 *Matter Radiat. at Extremes* **8** 028101
[15] Shvydko Y, Stoupin S, Blank V and Terentyev S 2011 *Nat. Photon.* **5** 539
[16] Gallin M L, Kim Y, Abbassi L, Bes A, Boiano C, Brambilla S, Collot J, Colombi G, Crozes T, Curtoni S, Dauvergne D, Destouches C, Donatini F, Gallin L, Ghouini O, Hostachy J Y, Iskra L, Jastrzab M, Kessedjian G, Lacoste A, Lyoussi A, Marcatili S, Motte J, Muraz J F, Nowak T, Ottaviani L, Pernot J, Portier A, Rahajandraibe W, Ramdhane M, Rydygier M, Sage C, Tchoualack A, Tribouilloy L and Yamouni M 2021 *Front. Phys* **9** 732730
[17] Ueno K, Tadokoro T and Ueno Y 2019 *Jpn. J. Appl. Phys.* **58** 106509
[18] Cui J M, Chen X D, Fan L L, Gong Z J, Zou C W, Sun F W, Han Z F and Guo G C 2012 *Chin. Phys. Lett.* **29** 036103

[19] Nordlund K, Zinkle S J, Sand A E, Granberg F, Averback R S, Stoller R E, Suzudo T, Malerba L, Banhart F, Weber W J, Willaime F, Dudarev S L and Simeone D 2018 *J. Nucl. Mater.* **512** 450

[20] Wang Y, Lai W S and Li J H 2020 *Chin. Phys. Lett.* **37** 016103

[21] Liu Y, Wang G, Wang S C, Yang J H, Chen L A, Qin X B, Song B, Wang B Y and Chen X L 2011 *Phys. Rev. Lett.* **106** 087205

[22] Wang K Y, Steeds J W, Li Z H and Wang H X 2017 *Appl. Phys. Lett.* **110** 152101

[23] Wang B, Xiong Y, Xia L S, Zhang H, Zhang K Z and Meng X Q 2011 *Diam. Relat. Mater.* **20** 433

[24] Hickey D P, Jones K S and Elliman R G 2009 *Diam. Relat. Mater.* **18** 1353

[25] Ardalkar R M, Salunkhe Y D, Gaonkar M P, Mane S N, Ghaisas O A, Desai S N and Reddy A V R 2024 *J. Min. Inst.* **266** 179

[26] Salustro S, Nöel Y, M. Z C, Olivero P and Dovesi R 2016 *J. Chem. Phys.* **145** 184701

[27] Laidlaw F, Beanland R, Fisher D and Diggle P L 2020 *Acta Mater.* **201** 494

[28] Guo F Y, Chen B, Zeng Q Y, Yu X X, Chen K G, Kang D D, Du Y, Wu J H and Dai J Y 2023 *J. Chem. Phys.* **159** 1089

[29] Zeng Q Y, Chen B, Zhang S, Kang D D, Wang H, Yu X X and Dai J Y 2023 *npj Comput. Mater.* **9** 213

[30] Wang H, Guo X, Zhang L, Wang H and Xue J 2019 *Appl. Phys. Lett.* **114** 244101

[31] Liu J H, Byggmästar J, Fan Z Y, Qian P and Su Y Y 2023 *Phys. Rev. B* **108** 054312

[32] Li Y, Kang D D, Dai J Y and Wang L W 2024 *npj Comput. Mater.* **10** 115

[33] Li W, Zhao H, Zeng X G, Yang X, Chi M H and Gao Y P 2025 *Nucl. Instrum. Methods Phys. Res. B* **559** 165608

[34] Wang W L, Wang K and Deng W J 2024 *Int. J. Mod. Phys. B* **38** 2450219

[35] Yu L T, Fan C, Gao Q Z and Lv L X 2024 *J. Phys. Conf. Ser.* **2882** 012088

[36] Fu B, Fitzgerald S, Hou Q, Wang J and Li M 2017 *Nucl. Instrum. Methods Phys. Res. B* **393** 169

[37] Robinson M, Marks N, Whittle K and Lumpkin G 2012 *Phys. Rev. B* **85** 104105

[38] Guo P F, Song C Z, Wu Y N and Chen S Y 2024 *Adv. Electron. Mater* **10** 2400014

[39] Wang D, Gao N, Setyawan W, Kurtz R J, Wang Z G, Gao X, He W H and Pang L L 2016 *Chin. Phys. Lett.* **33** 096102

[40] Norgett M, Robinson M and Torrens I M 1975 *Nucl. Eng. Des* **33** 50

[41] Ziegler J F, Ziegler M D and Biersack J P 2010 *Nucl. Instrum. Methods Phys. Res. B* **268** 1818

[42] Wu W and Fahy S 1994 *Phys. Rev. B* **49** 3030

[43] Zhou Y, Chen B, He H Y, Li B and Wang X L 2020 *Nucl. Technol.* **206** 32

[44] Holmström E, Nordlund K and Kuronen A 2010 *Phys. Scr.* **81** 035601

[45] Erginsoy C, Vineyard G and Englert A 1964 *Phys. Rev.* **133** A595

[46] Delgado D and Vila R 2011 *J. Nucl. Mater.* **419** 32

[47] Jin Y N, Huang H, Zhong Y H, Yuan X T, Li H, Lou D, Xie K, Liu Z X, Cai B and Peng Q 2022 *Ceram. Int.* **48** 16813

[48] Buchan J T, Robinson M, Christie H J, Roach D L, Ross D K and Marks N A 2015 *J. Appl. Phys.* **117** 245901

[49] Liu T, Shao T, Lyu F, Lai X and Shen A H 2022 *Model. Simul. Mater. Sci. Eng.* **30** 035005

[50] Delgado D and Vila R 2011 *J. Nucl. Mater.* **419** 32

[51] Devanathan R, Diaz de la Rubia T and Weber W J 1998 *J. Nucl. Mater.* **253** 47

[52] Ziegler J F and Biersack J P 1985 *The Stopping and Range of Ions in Matter* (Boston: Springer) p. 93

[53] Stukowski A 2009 *Model. Simul. Mater. Sci. Eng.* **18** 015012

[54] Saada D, Adler J and Kalish R 1999 *Phys. Rev. B* **59** 6650

[55] Prins J, Derry T and Sellschop J 1986 *Phys. Rev. B* **34** 8870

[56] Koike J, Parkin D and Mitchell T 1992 *Appl. Phys. Lett.* **60** 1450

[57] Robinson M, Marks N A and Lumpkin G R 2012 *Phys. Rev. B* **86** 134105

[58] Brenner D W and Shenderova O A 2015 *Phil. Trans. R. Soc. A.* **373** 20140139

[59] Slepetz B K, Miklos 2014 *Phys. Chem. Chem. Phys.* **16** 1515

[60] Mainwood A 1999 *Diam. Relat. Mater.* **8** 1560

[61] Setyawan W, Nandipati G, Roche K J, Heinisch H L, Wirth B D and Kurtz R J 2015 *J. Nucl. Mater.* **462** 329

[62] Fu J, Chen Y C, Fang J Z, Gao N, Hu W Y, Jiang C, Zhou H B, Lu G H, Gao F and Deng H Q 2019 *J. Nucl. Mater.* **524** 9